Accepted Manuscript

New device for the simultaneous measurement of diffuse solar irradiance on several azimuth and tilting angles

Miguel Simón-Martín de, Montserrat Díez-Mediavilla, Cristina Alonso-Tristán, David González-Peña
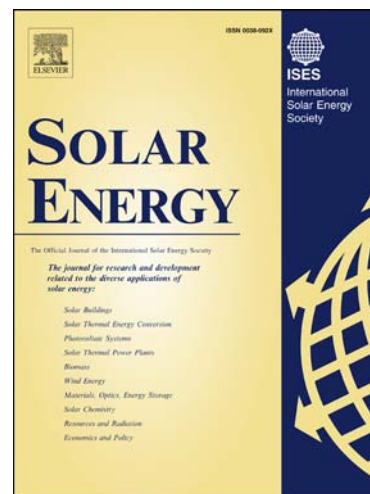
Please cite this article as: Simón-Martín, M. de, Díez-Mediavilla, M., Alonso-Tristán, C., González-Peña, D., New device for the simultaneous measurement of diffuse solar irradiance on several azimuth and tilting angles, *Solar Energy* (2015), doi: http://dx.doi.org/10.1016/j.solener.2015.06.001

New device for the simultaneous measurement of diffuse solar irradiance on several azimuth and tilting angles

Miguel de Simón-Martín[1], Montserrat Díez-Mediavilla, Cristina Alonso-Tristán, David González-Peña

Solar and Wind Feasibility Technologies Research Group. University of Burgos (Spain). E.P.S. Campus de Río Vena s/n, 09006.
miguel.simon@unileon.es, mdmr, catristan, davidgp @ubu.es

Abstract

A device is proposed for the measurement of diffuse solar irradiance on tilted surfaces pointing-to as well as fixed on the equatorial direction. Most commercial devices are not designed for this purpose. Here, we present a specific design for a system based on a single multi-lobe shadow-ring that allows us to measure diffuse irradiance with several tilted pyranometers -from 60 to 90 degrees from the horizontal plane- and on different azimuth angles. This first prototype allows us to measure in the four cardinal directions. The ring is designed to minimize the covered celestial dome observed by each sensor. Moreover, the complete device needs a very small installation area and its simplicity means it is inexpensive and easy to operate. The measurements have subsequently to be corrected with a geometrical correction factor that takes into account the portion of the sky vault blocked by the shadow-ring. These measurements are essential for estimating solar potential on tilted surfaces –such as building façades– and for improving current anisotropic solar models, among many other applications.

Keywords: Solar diffuse irradiance, shadow-ring, tilted surfaces, oriented surfaces, pyranometer, building integration, solar architecture.

1. Introduction

Global solar irradiance that incides on the Earth's surface is the sum of three components: beam, diffuse and reflected or albedo's irradiance [1]. The first component refers to the amount of energy that arrives straight-on in a line –the measured region, called the circumsolar region, is a solid angle of 1 str– from the Sun. Diffuse irradiance is the part of the solar energy that has been reflected and scattered in the atmosphere. Part of the irradiance returns to outer space and another part reaches the ground, the proportion of which depends on the size, density and characteristics of the chemical and aerosol particles present in the atmosphere. The final component is irradiance that is reflected from other elements on the horizon; diffuse irradiance, the measurement and estimation of which has yet to be properly developed. However, it is well established that the accurate assessment of diffuse irradiance is essential for estimating the

incidence of irradiance on different objects under real shadow conditions [2]. In addition to meteorological studies, solar irradiance data is used in many applications such as in architecture, engineering, agriculture and ecology [2, 3, 4]. Moreover, a deep knowledge of the distribution and characteristics of solar irradiance components is mandatory for improving the efficiency of solar collectors [5].

Currently, there are different instruments and methodologies for measuring solar diffuse irradiance, but most of them are only available to operate on horizontal or Equator pointed-to tilted surfaces [6]. In this paper, we present a new device that is capable, in an inexpensive and easy way, of measuring solar diffuse irradiance on several surfaces. The prototype that is presented can simultaneously measure diffuse irradiance on planes tilted from 60 to 90 degrees oriented towards the four cardinal directions: North, South, East and West.

The paper is organized into five further sections. The first one reviews the most commonly used devices for measuring solar diffuse irradiance in laboratories and solar plants across the world. In section 3, we summarize the geometrical analysis for simultaneously shad-

---

[1]Corresponding author: Department of Electric, Systems and Automatic Control Engineering. University of León (Spain). Campus of Vegazana s/n, 24071. Phone: +034 987 29 10 00 - 5391, e-mail: miguel.simon@unileon.es.

Nomenclature and abbreviations

d	Shadowband displacement mod.	[m]	R_p	Sensor dome radius	[m]
D_0	Diffuse horizontal irradiance	[W·m^{-2}]	r_x	x distance between lobe centers	[m]
D_c	Corrected diffuse measurement	[W·m^{-2}]	r_y	y distance between lobe centers	[m]
D_r	Registered diffuse measurement	[W·m^{-2}]	S	Sky dome fraction	[-]
e_x	x distance between sensors	[m]	V	Transverse angle	[rad]
e_y	y distance between sensors	[m]	W	Shadowband width	[m]
e_z	z distance between sensors	[m]		*Greek symbols*	
f_c	Geometrical correction factor	[-]	θ_{sp}	Sun-pyranometer angle	[deg]
G_0	Global horizontal irradiance	[W·m^{-2}]	θ_{zp}	Sensor tilting angle	[deg]
H_s	Solar time	[hr]	θ_{zr}	Shadow-ring tilting angle	[deg]
I_{gr}	Reflected irradiance	[W·m^{-2}]	θ_{zs}	Solar zenith angle	[deg]
I_r	Shadow-ring blocking irradiance	[W·m^{-2}]	δ_s	Solar declination angle	[deg]
I_{sky}	Irradiance from the sky dome	[W·m^{-2}]	γ_p	Sensor azimuth angle	[deg]
I_t	Irradiance on the sensor plane	[W·m^{-2}]	γ_r	Shadow-ring azimuth angle	[deg]
$K_{d,0}$	Horizontal diffuse fraction	[-]	γ_s	Solar azimuth angle	[deg]
N	Day of the year [1-365]	[day]	ω_s	Solar hourly angle	[deg]
L	Radiance	[W·m^{-2}·sr^{-1}]	ω_0	Daylight duration angle	[deg]
L_{sky}	Radiance from the sky dome	[W·m^{-2}·sr^{-1}]	λ	Shadow-ring yaw angle	[deg]
L_{gr}	Radiance from the ground	[W·m^{-2}·sr^{-1}]	ψ	Shadow-ring width-radius ratio	[-]
R	Shadow-ring's lobe radius	[m]	ρ	Ground isotropic reflectance	[-]

owing different pyranometers. We then describe the proposed prototype and its components in section 4. In section 5, the expression of the geometrical correction factor needed to adjust the obtained measurements due to the interference of the shadowband is shown. Finally, the main conclusions on the proposed device are explained in the last section.

2. Measuring diffuse solar irradiance

The bibliography offers several works on instruments designed to measure solar diffuse irradiance on a horizontal surface or facing the direction of the Equator [1, 6, 7]. Nowadays, the most popular are Drummond's shadowring -also called shadowband-, the rotating shadowband pyranometer, and the tracking solar disk.

Drummond's shadowring is a practical and widely used approach to measure solar diffuse irradiance, which consists of a metal band that blocks the Sun's path along the sky dome [8, 9, 10]. It is an easy-to-operate stationary device that, although it can be automatized, is usually manually adjusted by sliding the ring every few days, depending on the latitude of the mounting place. The shadowband describes a ring which is usually tilted along the same angle as the latitude. By doing so, the ring only has to be adjusted according to the decline of the sun. A commercial example is shown in Fig. 1.

Figure 1: Commercial example of Drummond's shadow-ring [11].

2

On the other hand, the rotating shadowband pyranometer [12, 13, 14] has a motorized partial ring which rotates through a latitude tilted axis from sunrise to sunset (see Fig. 2) to block beam irradiance.

Figure 2: Commercial example of rotating shadowband [15].

Finally, the tracking solar disk shades the pyranometer with a small disk or ball synchronized with the Sun's apparent motion in the sky (e.g. Fig. 3). It minimizes the shadowing element, thus many authors consider its correction factor almost negligible. However, this technique is much more expensive, requires much more maintenance and can be unstable under strong winds.

Some studies confirm that measurements with shadow-rings are comparable to those given by more sophisticated tracking devices under totally cloudy skies, while some differences appear under clear sky conditions [10, 9, 17]. This phenomenon can be explained due to the anisotropy effects in the atmosphere and they can be corrected by applying different correction models, supplementary to the geometrical correction model.

Other ways to measure solar diffuse irradiance exist, which are less common due to their complexity, costs or low performance rates. Just to give a few examples, we can find modified versions of Drummond's shadow-ring, such as the one presented by de Oliveira, A.P. et al. [18], which can be seen in Fig. 4. Instead of adjusting the shadow-ring, it is fixed to the mounting structure and the pyranometer slides over a horizontal plane along the

Figure 3: Commercial example of tracking solar disk [16].

Figure 4: Oliveira's shadow-ring device [18].

3

North-South direction depending on the day of the year. Another method can be seen in patent WO2011/139279 [19], which introduces a device that measures diffuse irradiance by comparing the outputs of several sensors positioned on an horizontal plane. An opaque cylinder placed in the center of the device shadows a few of the sensors. The diffuse irradiance value is then calculated as the minimum of the registered measurements.

One of the few devices that is able to measure diffuse irradiance in several directions as well as the North-South one, is the spectral sky-scanner. This sort of device allows researchers to measure sky vault luminance with a sensor that takes spectral measurements in a broader range of the electromagnetic spectrum [7]. So, diffuse irradiance can be computed [20]. These devices are usually based on a sensor with a vision angle of about 10 deg. which rotates around two orthogonal axes, like the one described in [21]. Another prototype version has been developed by the University of Paderborn[22] that uses over 100 silicon sensors oriented around a radial distribution.

3. Shadowband fundamentals

In this section, we introduce the fundamental aspects of the device that is presented. Our aim is to shadow multiple pyranometers simultaneously, with different azimuth and tilting angles, thereby reducing measurement aberrations and associated costs. The result is one single multi-lobe shadow-ring, with as many rounded parts as solar sensors. This section is divided into two parts. In the first, we show the geometrical conditions for shadowing a single pyranometer. In the second, we explain the procedure by which those geometrical restrictions are extrapolated to multiple sensors.

3.1. Geometrical analysis for one pyranometer

The Sun path in the sky dome has to be blocked when observed by one pyranometer. This movement has been widely studied [1] and it can be defined by two horizontal coordinates: the zenith angle (θ_{zs}) and the azimuth angle (γ_s). The first measures the angle between the visual line of the Sun and the perpendicular line to the site observer. The second one measures the angle between the projection of the Sun's visual line and the equatorial direction. Fig. 5 shows a scheme with both coordinates which are respectively defined in eqs. (1) and (2).

$$\cos(\theta_{zs}) = \sin(\phi)\sin(\delta_s) + \cos(\phi)\cos(\delta_s)\cos(\omega_s) \quad (1)$$

$$\tan(\gamma_s) = \frac{\cos(\delta_s)\sin(\omega_s)}{\cos(\delta_s)\sin(\phi)\cos(\omega_s) - \sin(\delta_s)\cos(\phi)} \quad (2)$$

where ϕ is the latitude of the observer's geographic location, δ_s is the Sun's declination angle and ω_S is the hourly angle.
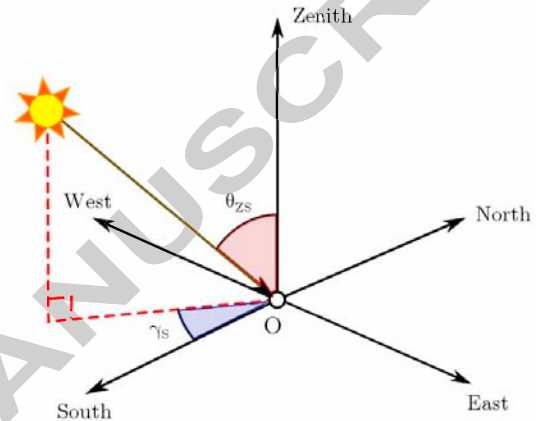

Figure 5: Horizontal coordinates describing the position of the Sun.

The declination angle of the Sun in [deg] can be defined by the following expression:

$$\delta_s = 23.45\sin\left(360\frac{284 + N}{365}\right) \quad (3)$$

where N is the day of the year ($N \quad [1, 365], N \quad \mathbb{N}$).

The hourly angle depends on the solar time (H_s) as it can be seen in equation (4).

$$\omega_s = 15(H_s - 12) \quad (4)$$

As the observed sky dome has a semispherical shape, the optimum geometry for shadowing one single pyranometer must be a spherical section, which can be approximated by a cylindrical section or ring. Thus, the borders or the shadowband can be described by Cartesian coordinates that refer to the center point of the shadowband $Q = [X_Q, Y_Q, Z_Q]$ as in:

$$\begin{pmatrix} X \\ Y \\ Z \end{pmatrix} = \begin{pmatrix} R\cos(\chi) \\ R\sin(\chi) \\ \pm\dfrac{W}{2} \end{pmatrix} \quad (5)$$

This shadow-ring is placed in a relative position to the sensor (the center point of which is $O = [X_O, Y_O, Z_O]$), which can be split into a displacement, described by

4

vector **d**, and rotations along three orthonormal axes, described by a rotation matrix **M**.

The displacement vector **d** is the sum of the displacements along the x, y and z axes. As the Sun's path in the sky dome is symmetrical to the observer's *"Meridian Plane"*, displacement along the y axis is null if we align the device in the North-South direction.

$$\mathbf{d} = \mathbf{d_x} + \mathbf{d_z} = \begin{pmatrix} X_Q - X_O \\ 0 \\ Z_Q - Z_O \end{pmatrix} \qquad (6)$$

The rotation matrix **M** is the product of the rotation matrix on each axis of Euler's rotation angles: "pitch", "yaw" and "roll". Due to the symmetry with the North-South direction, rotation on the x axis is null. Moreover, as the band shape has axial symmetry, any rotation on the z axis will change the observed curve. Thus, the rotation matrix is in this case reduced to:

$$\mathbf{M}(\lambda_1, \lambda_2, \lambda_3) = \mathbf{M_y}(\lambda) = \begin{pmatrix} \cos(\lambda) & 0 & \sin(\lambda) \\ 0 & 1 & 0 \\ -\sin(\lambda) & 0 & \cos(\lambda) \end{pmatrix} \qquad (7)$$

Finally, a general equation of the shadowband in absolute Cartesian coordinates that refer to the sensor center point O is:

$$\begin{pmatrix} X \\ Y \\ Z \end{pmatrix} = \mathbf{M}(\lambda) \times \begin{pmatrix} X \\ Y \\ Z \end{pmatrix} + \mathbf{d} \qquad (8)$$

We can transform the Cartesian coordinates into horizontal ones by:

$$\cos(\theta_{zr}) = -\frac{Z}{X^2 + Y^2 + Z^2} \qquad (9)$$

$$\tan(\gamma_r) = \frac{Y}{X} \qquad (10)$$

The shadowband results are parametrized by the following variables: radius (R), width (W), tilting angle (θ_{zr}) and the displacement (**d**) between the ring center Q and the sensor O. These variables must be optimized for optimal performance of the shadow-ring.

We know that the path of the Sun in the sky dome is the intersection of the *"Ecliptic Plane"* with the sky dome. This plane cuts through the Earth's orbit around the Sun and it is tilted with reference to the *"Celestial Equator Plane"* (which cuts through the Equator) or declination angle. As the Earth only moves its orbit and does not rotate, the declination angle changes throughout the year by equation (3) [23]. Thus, the Celestial Equator plane is the mid-position of the path of

the Sun in the sky dome. We may immediately infer that the best tilting angle for the shadowband is complementary to the latitude angle ($\theta_{zr} = \pi/2 - \phi$), which makes the shadowband plane parallel to the Celestial Equator Plane, as it can be seen in Fig. 6. So, the yaw angle of the rotation matrix must be:

$$\lambda = -\theta_{zr} = \phi - \frac{\pi}{2} \qquad (11)$$

So as to shadow the sensor center point O throughout the whole year, the shadowband width (W) of a fixed ring must comply with:

$$W = 2R \tan\left[\max\left(\delta_s\right)\right] \qquad (12)$$

However, this width value means that the ratio:

$$\psi = \frac{W}{R} \qquad (13)$$

is unacceptable to achieve a low shadowband aberration value on a clear-sky diffuse irradiance measurement. The solution is therefore found by decreasing the shadowband width to an acceptable value and shifting the shadowband throughout the year in accordance with the declination angle.
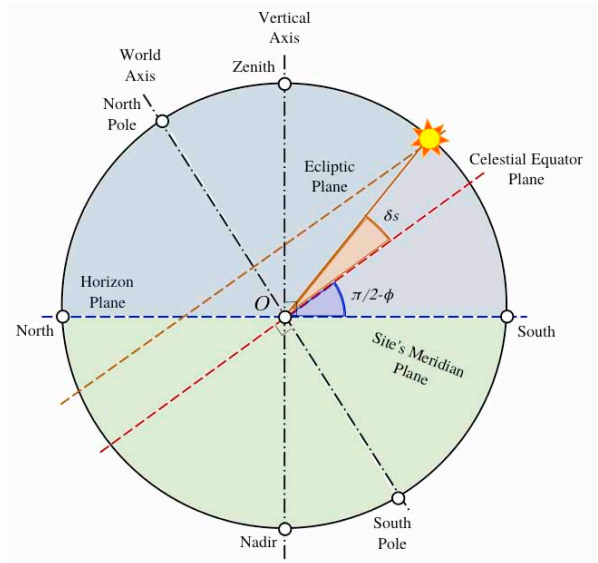

Figure 6: Sky dome reference planes.

The Ecliptic Plane is always parallel to the Celestial Equatorial Plane, which is tilted to the observer's *"Horizon Plane"* (perpendicular to the observer vertical axis) or latitude angle [23]. Thus, the shadowband center point Q must displace along a perpendicular axis

to that plane that also contains the sensor reference point O. Then, the displacement vector must be:

$$\mathbf{d} = \mathbf{d_x} + \mathbf{d_z} = \begin{pmatrix} -d\cos(\phi) \\ 0 \\ d\sin(\phi) \end{pmatrix} \qquad (14)$$

where d is the modulus of the displacement vector and its value must agree with:

$$d = R\tan(\delta_s) \qquad (15)$$

Finally, the shadow-ring width must be calculated, in order to project shadow through the dome of the complete sensor over the whole year. Thus, the shadowband width must agree with:

$$\frac{W}{2R_p} \geq \max\left[\frac{\cos(\delta_s + \phi - \theta_{zp})}{\cos(\delta_s)}\right] \qquad (16)$$

where θ_{zp} is the sensor tilting angle referred to the vertical axis and R_p is the dome radius of the sensor. We can check the evolution of this function throughout the year in Fig. 7.
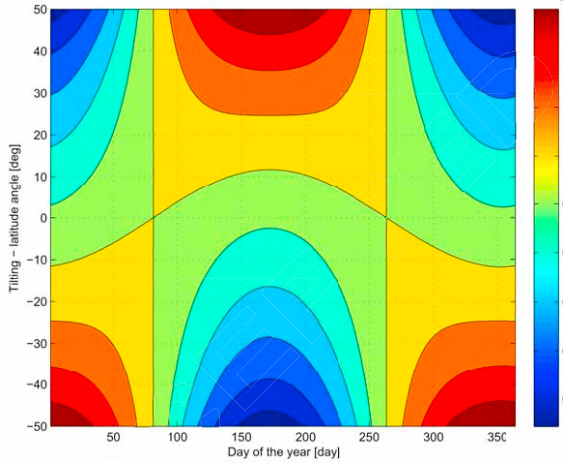

Figure 7: Shadowing ratio analysis.

So, the shadowband radius is defined by equation (13) the value of which for most commercial devices is in the range of $[0.15, 0.25]$: the larger this ratio, the larger the measured error and the geometrical correction factor (see section 5).

3.2. Shadowing four pyranometers simultaneously

Once we know the geometrical properties that the shadow-ring should have to adequately block the Sun's path observed by one pyranometer, our aim is to extend the simple pyranometer case simultaneously to several sensors. We have seen in the previous subsection that the optimum geometry for the shadowband is a cylinder section. Thus we should find the way for the shadow ring of each sensor to have the same properties. A solution has been found in a multi-lobe shadow-ring with as many (cylindrical) lobes as pyranometers. Moreover, if we want to have one single flat shadowband, we should place the pyranometers in certain positions. Those positions are defined by the intersection of a parallel plane to the shadowband through a reference point. In this case we decided to choose the center of the support structure as the reference point. Thus, the pyranometers facing East and West pyranometers are placed in the center of the corresponding sides of the structure and the sensors pointing North and South should be placed at a similar height (e_z) to the pyranometers facing East-West:

$$e_z = e_y\tan(\theta_{zr}) \qquad (17)$$

where e_y is the distance between pyranometers in the y axis (see Fig. 8).
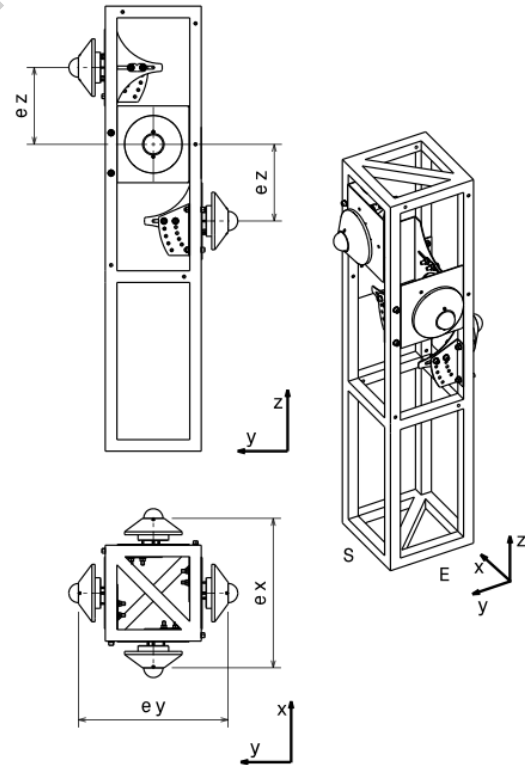

Figure 8: Sensors positions in the supporting structure.

As we can see in Fig. 9 lobes center points Q_i in the multi-sensors shadowband are in the same plane and
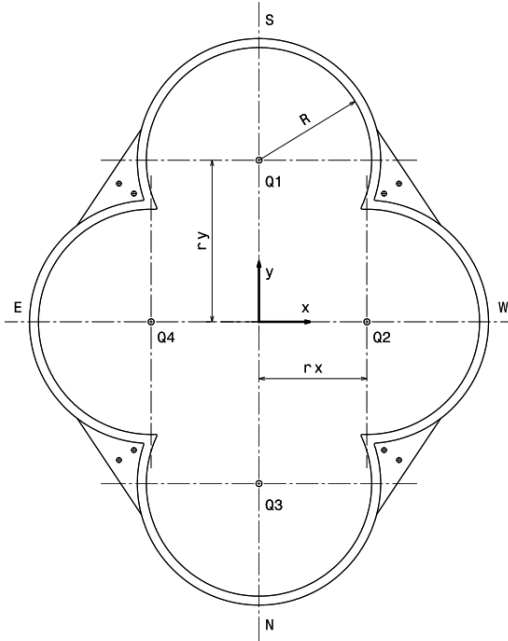
Figure 9: Multilobes designed shadowband for 4 sensors.

separated from the shadowband center distances r_x and r_y in the x and y axes, respectively, defined by equations (18) and (19).

$$r_x = e_x \tag{18}$$

$$r_y = \frac{e_y}{\cos(\theta_{zr})} \tag{19}$$

Moreover, in order to guarantee that each sensor has a 180 deg field-view angle, each lobe must be checked (in case $r_y \geq r_x$):

$$\arctan\left(\frac{r_y}{r_x}\right) + \arctan\left(\sqrt{\frac{4R^2}{r_x^2 + r_y^2} - 1}\right) \leq \frac{\pi}{2} \tag{20}$$

4. Prototype description

Applying the theoretical analysis described in the previous section, we have developed a real prototype which is able to measure solar diffuse irradiance on planes facing the four main cardinal directions –East, South, West and North– and with different tilting angles –from 60 deg. to 90 deg.–. This new device, depicted in Figs. 10 and 11, is composed of a prismatic frame of 1160 mm in height which supports all sensors, several

mechanisms for tilting the pyranometers and a multi-lobe -4 lobe- shadow-ring, which is adjusted by a single transverse bar that slides through two cylinders mounted on two lateral plates fixed to the main frame.

Figure 10: Prototype perspective front view.

The main frame is made of laminated square bars of inox. steel with a 30 mm square edge section. It is fixed to a concrete base by screws and it is robust enough to face high speed wind forces. On the top and on the bottom it has two crossing bars in opposite directions to avoid sectional deformations.

Four tilting mechanisms can be found screwed to the frame. These mechanisms support the pyranometers and they have two components. The first one is a plate screwed to the steel frame, which, in this case, allows 5 different tilting positions between 60 deg. and 90 deg. The second one is another plate with an "L" shape, which is linked to the previous one by two screws that can slide through an edge. This system allows us to mount pyranometers from different manufacturers -the sensor's surface height from the base can measure from 26up to 98 mm-. It is mandatory to adjust the sensor to a satisfactory position, in order to put the actinometer's sensing surface (reference point O_i) in a satisfactory position in relation to the reference point Q_i of the
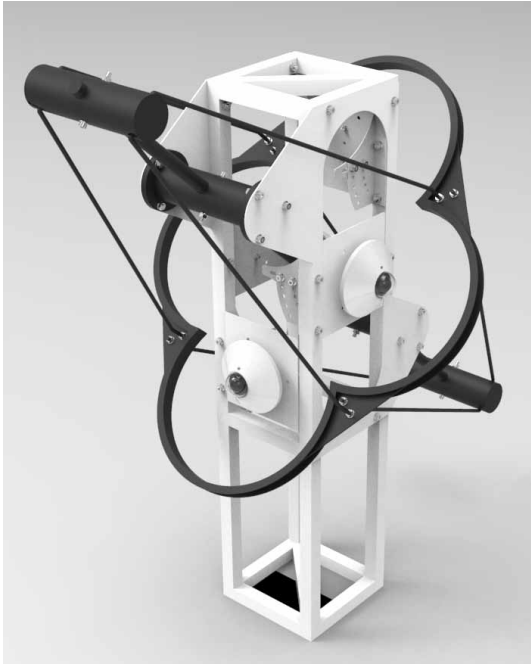
7

Figure 11: Renderized prototype perspective rear view.

Figure 12: Shadowband detail in the renderized prototype.

shadow-ring.

Moreover, two plates are screwed onto both sides of the frame –East and West–. These plates support two cylinders between them with four steel rings with widths of 20 mm. These cylinders allow a transverse bar slide through a latitude tilted axis and adjust the position of the multilobes shadowband throughout the year, to correct the Sun's declination variance. As we can see in Fig. 12 the shadowband has a "U" section which makes the transverse angle seen by the pyranometer far more stable in relation to the angle variance of the Sun. Furthermore, this section profile makes the shadowband stronger and much more rigid. The multilobe shadowband is fixed to the sliding bar by eight steel bars screwed to four plates that are welded to the intersections of the lobes.

A real prototype is currently functioning on the rooftop of the EPS of the University of Burgos (see Fig. 13). Table 1 summarizes the SWOT (Strengths, Weaknesses, Opportunities and Threats) of the device that is depicted. This sort of analysis are widely used in the product design industry and allow us to state a project according to its internal (strengths and weaknesses) and external (opportunities and threats) properties.

From SWOT analysis shown in Table 1 we want to highlight the application of the obtained measurements

Figure 13: Real prototype perspective front view.

8

Table 1: SWOT analysis of the MK prototype.

Strengths
Simultaneous measurements.
Low-maintenace needs.
Low-cost structure.
Easy to operate.
Available automatic control.
High wind efforts resistance.
Scalable to several sensors.

Weaknesses
Several pyranometers needed.
Geographically dependent design.
Restricted maximum number of sensors.
Geometric correction factor calculation.

Opportunities
Building Integrated Photovoltaic Systems.
Improved spatial distribution irradiance models are widely needed.
Irradiance studies on urban environments to improve lightning policies.

Threats
Increased use of sky-scanners in laboratories.
Good data sets need long-term data measurment campaigns.

in improving BIPV systems and its simulations, such as in [24, 25, 26, 27].

5. Geometrical correction factor

A pyranometer equipped with a shadow ring measures the solar diffuse irradiance that achieves the Earth's surface on a plane in a solid angle of 2π sr, with the exception of the solid angle blocked by the shadow-ring [28, 29]. The reflectance of the internal part of the shadowband is considered negligible. Thus, it results mandatory to apply, at least, a geometrical correction factor f_c to correct the error due to the unseen sky dome. This factor can be defined as:

$$\frac{D_c}{D_r} = \frac{2\pi}{2\pi - x} = \frac{1}{1 - \dfrac{x}{2\pi}} = \frac{1}{1 - S} = f_c \qquad (21)$$

where D_c is the corrected diffuse value, x is the solid angle measured in [sr] blocked by the shadowring and D_r is the recorded diffuse value by the sensor. S is the fraction of the diffuse irradiance intercepted by the shadowband.

S can be defined as the ratio between the irradiance intercepted by the shadowband (I_r) and the total irradiance incident on the pyranometer plane (I_t):

$$S = \frac{I_r}{I_t} = \frac{I_{r,sky} + I_{r,gr}}{I_{t,sky} + I_{t,gr}} \qquad (22)$$

where *"sky"* subindex refers to the open sky part viewed by the pyranometer, and *"gr"* subindex is related to the ground reflected measured irradiance, also called albedo's irradiance. According to [30] both radiances are related by the following expression:

$$L_{gr} = \frac{\rho G_0}{\pi} = \frac{\rho \left(D_0/K_{d,0} \right)}{\pi} = \frac{\rho}{K_{d,0}} L_{sky} \qquad (23)$$

where ρ is the isotropic reflectivity of the surrounding ground, G_0 is the global irradiance on the horizontal plane, D_0 is the diffuse irradiance on the horizontal plane and $K_{d,0}$ is the horizontal diffuse fraction.

Each differential part of the irradiance from the sky vault blocked by the shadow-ring can be expressed by:

$$dI_r = L \cos(\theta_{sp}) V \cos(\delta_s) d\omega \qquad (24)$$

where θ_{zp} is the angle between the Sun position on the sky dome and the pyranometer –see equation (25) [31]–, V is the transverse angle observed by the pyranometer – which depends on the geometry of the blocking element – and ω is the hourly angle measured on the shadow-ring medium plane. We must integrate the previous expression into two parts, depending on the pyranometer's azimuth angle and the part of the shadow-ring which blocks the incoming sky radiance ($L = L_{sky}$) and the part which blocks the ground reflected one ($L = L_{gr}$). The intersection of the Ecliptic Plane with the Horizon, measured in hourly coordinates in the shadow-ring medium plane, is defined by equation (26) where ω_0 denotes the maximum hourly angle from the sunrise (or sunset) and noontime. This hourly angle defines the semi-daylight duration, and depends on the geographical latitude of the observer and the solar declination angle.

$$
\begin{aligned}
\cos(\theta_{sp}) = \ & \sin(\delta_s)\sin(\phi)\cos(\theta_{zp}) \\
& - \sin(\delta_s)\cos(\phi)\sin(\theta_{zp})\cos(\gamma_p) \\
& + \cos(\delta_s)\cos(\phi)\cos(\theta_{zp})\cos(\omega) \\
& + \cos(\delta_s)\sin(\phi)\sin(\theta_{zp})\cos(\gamma_p)\cos(\omega) \\
& + \cos(\delta_s)\sin(\theta_{zp})\sin(\gamma_p)\sin(\omega)
\end{aligned}
$$
$$(25)$$

$$\cos(\omega_0) = -\tan(\phi)\tan(\delta_s) \qquad (26)$$

We must notice that for certain latitudes close to the geographic poles, where $-\tan(\phi)\tan(\delta_s) > 1$, the Sun never cross the horizon and day or night lasts 24 hours. For those cases, ω_0 must be set to 1 or 0 according to the declination and latitude signs. It also can happen that

9

the pyranometer plane and the Ecliptic never intersects due to they are parallel planes. Equivalent correction must be done.

Finally, the transverse angle depends on the geometry of the shadowband. In this case, as the transverse section of the shadow-ring is a "U" profile, an acceptable approximation of the transverse angle value is:

$$V \approx 2 \sin \frac{V}{2} = \frac{W}{R + W \tan(\delta_s)/2} \approx \frac{W}{R} \qquad (27)$$

where W is the width of the shadow-ring and R is its internal radius.

In Figs. 14, 15 and 16 we have calculated the geometrical correction factor for each pointed-to pyranometer of the prototype device (Equator pointed-to, East or West facing and Pole pointed-to) in the case they are tilted 90 degrees (default tilting position).

Figure 15: Geometrical correction factor for an East or West facing pyranometer as a function of the latitude ϕ and day of the year N.
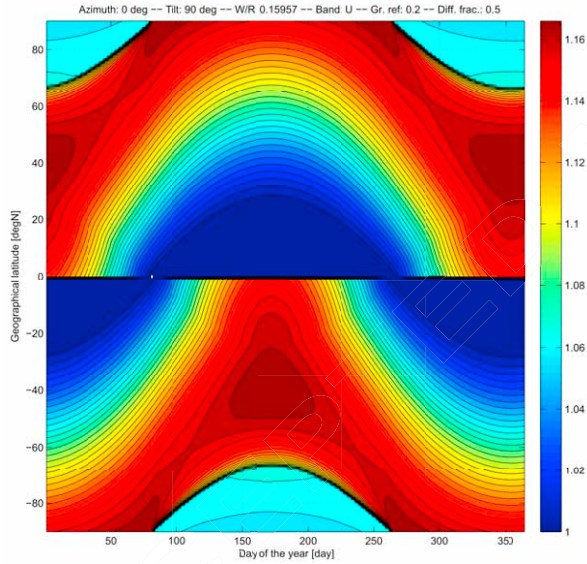

Figure 14: Geometrical correction factor for an Equator facing pyranometer (South pointed-to at the Northern Hemisphere) as a function of the latitude ϕ and day of the year N.

We have considered a ground reflectance value $\rho = 0.2$ and a diffuse fraction $K_d = 0.5$ remaining constant the whole year as an approximation. Both values are widely considered as mean ones in the literature [30, 31, 32, 33]. Real values must be applied in the case they are known or measured. We can see how it varies throughout the year depending on the pyranometer, geographic latitude and azimuth angles. We want to remark that Fig. 14 refers to an Equator pointed-to pyranometer, in other words, a South facing sensor in the Northern Hemisphere an a North facing one in the
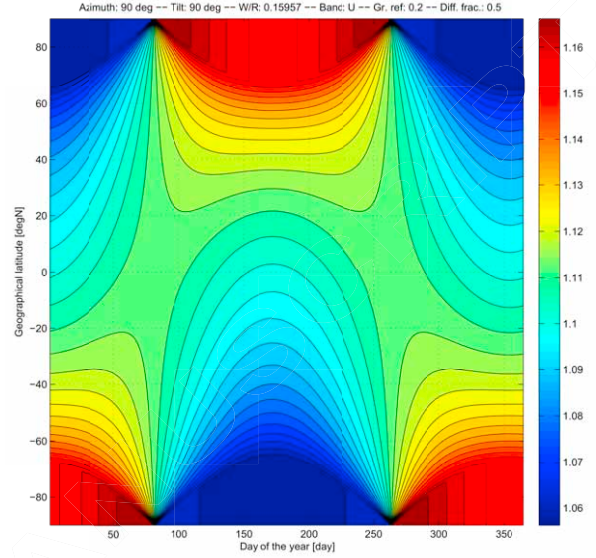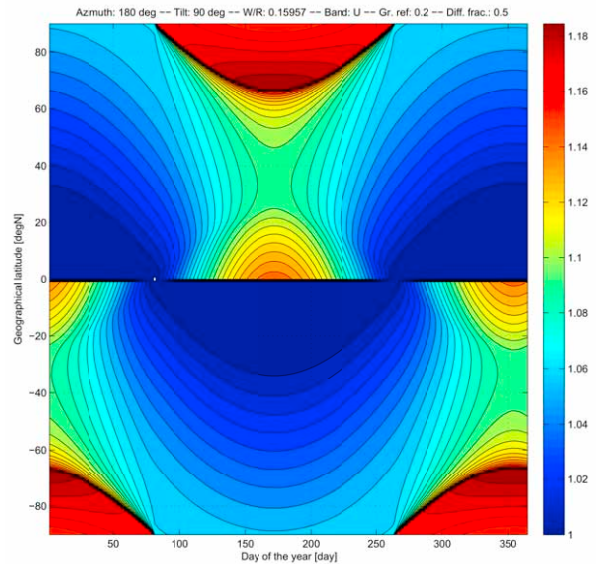

Figure 16: Geometrical correction factor for a Pole facing pyranometer (North pointed-to at the Northern Hemisphere) as a function of the latitude ϕ and day of the year N.
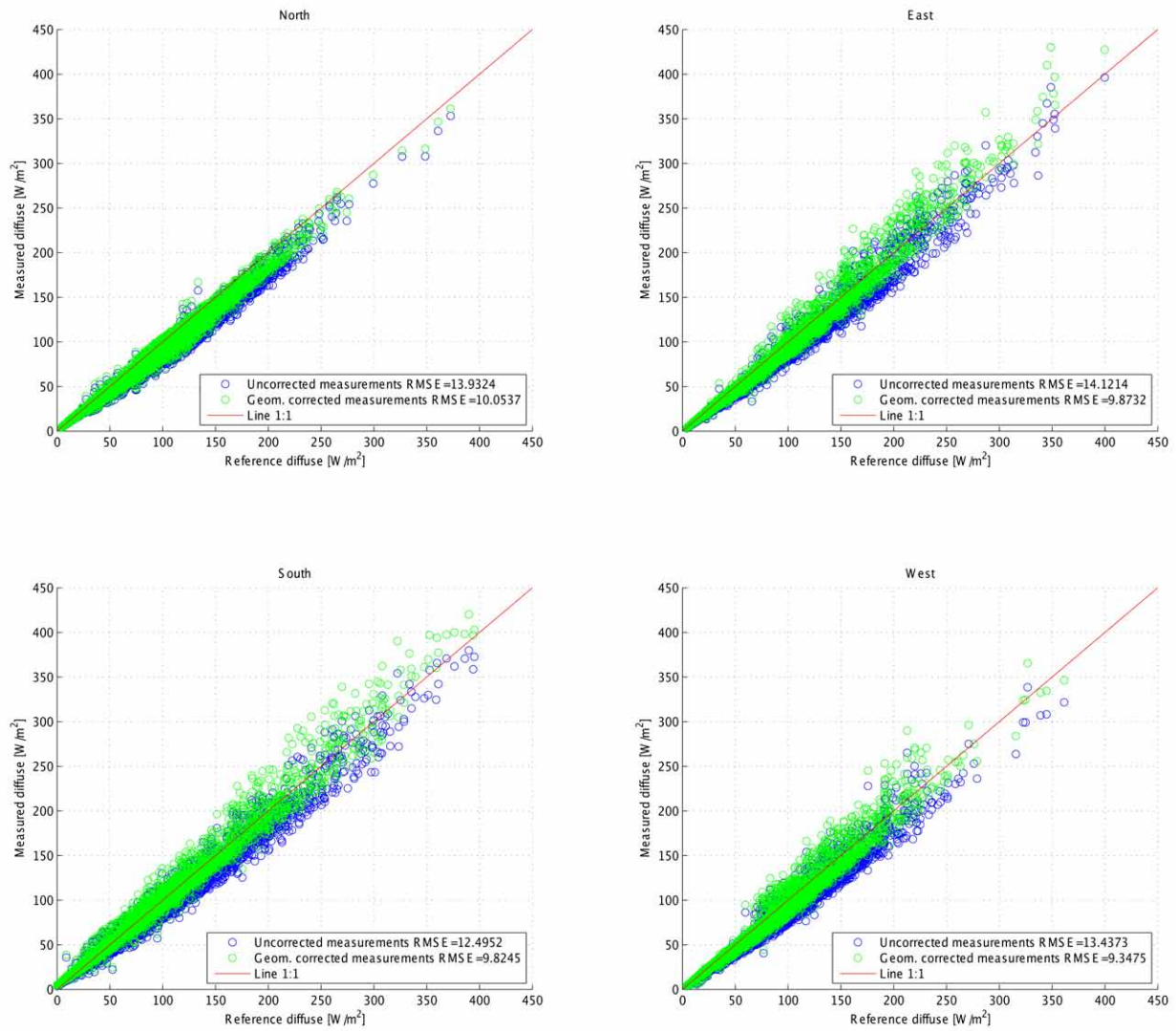
Figure 17: Preliminary results for the four cardinal directions measurements.

Southern Hemisphere. Analogous consideration must be done for Fig. 16 but with the geographical Poles.

The three colormaps for the geometrical correction factor shown in Figs. 14, 15 and 16 are symetric from the day of the year and inverse symmetric from the geographical latitude, as expected. We can detect inflection points at equinoxes and solstices and less variations on the f_c values at intermediate latitudes (from 30 to 60 degrees). In all cases $f_c \geq 1$ and its maximum value is less than 1.2 which means that the shadowband makes an error less than 20%.

We wish to remark that the calculated geometrical correction factor does not take into account any atmospherical anisotropic effects. Thus, if we want to improve measurement accuracy, we should in addition apply satisfactory adequate models [17, 28, 34, 35].

6. Preliminary results

On Fig. 17 we can see the preliminary measurements obtained by the built prototype currently functioning on the rooftop of the EPS of the University of Burgos. This device was installed in August 2014 and is fully operating since October 2014. Shown measurements correspond to the period from October 2014 to April 2015 with more than 10 000 datapoints recorded every 10 minutes as an average of every 1 second measurements, for each sensor. Rough measurements (blue points) and geometrically corrected ones (green points) are included in each graph, as well as the Root Mean Square Error ($RMSE$) for each dataset. The reference diffuse measurements have been obtained by subtracting the projected beam irradiance on each plane to the global measured irradiance on each cardinal direction, according to the three components model:

$$D = G - B\cos(\theta_{sp}) - R \qquad (28)$$

where D is the diffuse irradiance on the tilted plane, B is the beam irradiance measured by a pyrheliometer and R is the reflected irradiance. As the device does not include any reflected irradiance shield yet, this component has been included into the results.

Presented preliminary results show that the proposed device is quite accurate in all studied directions. Moreover, by applying the geometrical correction factor deduced for the device, $RMSE$ with the reference diffuse value decreases from a 21.37% for South facing measurements up to 30.44% for West facing ones respect to the uncorrected measurements. The average final $RMSE$ is less than 9.78 W/m². Deviations tend to increase with the diffuse value due to those measurements

correspond to clear sky conditions when anysotropic effects in the atmosphere are much more remarkable.

7. Conclusions

We have reviewed the instruments employed for the measurement of solar diffuse irradiance on the Earth's surface. It has been noted that most of these are only designed to measure this value on an horizontal plane or in a pointed-to North-South tilted direction. To check current diffuse solar distribution models or to develop new ones, it is mandatory to measure its value on different planes. So, we presented a new instrument for the simultaneous measurement of diffuse solar irradiance on several azimuth and tilting angles. The prototype that has been built allows us to measure this value on tilting angles from 60 to 90 degrees along the four cardinal directions with one single shadowband. The innovative aspect of this prototype is the multilobe shape of the shadow-ring and the relative positions between sensors. Although the instrument can be automatized it is easily to manually adjust by one single operator. Thus, it is inexpensive, easy to operate and it has low maintenance costs. However, as it is based on shadowband technology, calculation of a geometrical correction factor is needed to balance the measurements.

The Prototype design described in this paper is protected under Spanish Law (Patent P201400714).

References

[1] M. Iqbal, An introduction to solar radiation, Academic Press, California (USA), 1983.

[2] Z. Sen, Solar energy in progress and future research trends, Progress in Energy and Combustion Science 30 (4) (2004) 367–416, journal Article.

[3] P. C. Jain, Modelling of the diffuse radiation in environment conscious architecture: The problem and its management, Solar & Wind Technology 6 (4) (1989) 493–500. doi:10.1016/0741-983X(89)90064-7.

[4] J. Kanters, M. Horvat, Solar energy as a design parameter in urban planning, Energy Procedia 30 (2012) 1143–1152. doi:10.1016/j.egypro.2012.11.127.

[5] P. S. Koronakis, On the choice of the angle of tilt for south facing solar collectors in the Athens basin area, Solar Energy 36 (3) (1986) 217–225. doi:10.1016/0038-092X(86)90137-4.

[6] F. Vignola, J. Michalsky, T. Stoffel, Solar and Infrared Radiation Measurements, Vol. 1 of Energy and the Environment, CRC Press, Boca Raton, 2012.

[7] T. Muneer, Solar Radiation and Daylight Models, 2nd Edition, Vol. 1, ButterWorth-Heinemann, Oxford, 2004.

[8] A. J. Drummond, On the measurement of sky radiation, Archiv für Meteorologie, Geophysik und Bioklimatologie, Serie B 7 (3-4) (1956) 413–436. doi:10.1007/BF02242969.

[9] N. Robinson, L. Stoch, Sky Radiation Measurement and Corrections, Journal of Applied Meteorology 3 (2) (1964) 179–181. doi:10.1175/1520-0450(1964)003.

[10] A. J. Drummond, Comments on Sky Radiation Measurement and Corrections, Journal of Applied Meteorology 3 (6) (1964) 810–811. doi:10.1175/1520-0450(1964)003.

[11] Kipp and Zonen, CM 121 Shadow Ring (2014).
URL http://www.kippzonen.com/Product/42/CM-121B-C-Shadow-Ring#.VKEkwED4cLA

[12] J. J. Michalsky, R. Perez, R. Stewart, B. A. LeBaron, L. Harrison, Design and development of a rotating shadowband radiometer solar radiation/daylight network, Solar Energy 41 (6) (1988) 577–581. doi:10.1016/0038-092X(88)90060-6.

[13] R. D. Little, Rotating shadowband pyranometer, international Classification G01J1/04, G01J1/42 (Feb. 2005).

[14] J. J. Michalsky, J. A. Augustine, P. W. Kiedron, Improved broadband solar irradiance from the multi-filter rotating shadowband radiometer, Solar Energy 83 (12) (2009) 2144–2156. doi:10.1016/j.solener.2009.08.007.

[15] Irradiance, Rotating Shadowband Radiometer (2014).
URL http://www.irradiance.com/rotating-shadowband-radiometer

[16] Kipp and Zonen, Solys 2. 2-Axis Sun Tracker (2014).
URL http://www.kippzonen.com/Product/20/SOLYS-2-Sun-Tracker#.VKEka0D4cLA

[17] G. Sánchez, A. Serrano, M. L. Cancillo, J. A. Garc´a, Comparison of shadow-ring correction models for diffuse solar irradiance, Journal of Geophysical Research: Atmospheres 117 (D9). doi:10.1029/2011JD017346.

[18] A. P. de Oliveira, A. J. Machado, A New Shadow-Ring Device for Measuring Diffuse Solar Radiation at the Surface, Journal of Atmospheric and Oceanic Technology 19 (2001) 698–708.

[19] G. Burba, Direct, diffuse, and total radiation sensor, international Classification G01D5/34, G01J1/16, G01J5/02 (Nov. 2011).
URL http://www.google.st/patents/WO2011139279A1

[20] L. Kómar, A. Rusnák, R. Dubnicka, Analysis of diffuse irradiance from two parts of sky vault divided by solar meridian using portable spectral sky-scanner, Solar Energy 96 (2013) 1–9. doi:10.1016/j.solener.2013.07.003.

[21] Eko instruments, Eko Sky Scanner MS-321LR (2015).
URL http://eko-eu.com/products/solar-radiation-and-photonic-sensors/sky-scanner

[22] Voss, Jurgen, Der Solar Igel (2015).
URL http://www.solarigel.de/

[23] R. Green, Spherical Astronomy, Cambridge University Press, 1985.

[24] S.-H. Yoo, Simulation for an optimal application of BIPV through parameter variation, Solar Energy 85 (7) (2011) 1291–1301. doi:10.1016/j.solener.2011.03.004.

[25] F. Azadian, M. A. M. Radzi, A general approach toward building integrated photovoltaic systems and its implementation barriers: A review, Renewable and Sustainable Energy Reviews 22 (2013) 527–538. doi:10.1016/j.rser.2013.01.056.

[26] C. Catita, P. Redweik, J. Pereira, M. C. Brito, Extending solar potential analysis in buildings to vertical facades, Computers & Geosciences 66 (2014) 1–12. doi:10.1016/j.cageo.2014.01.002.

[27] S. Freitas, C. Catita, P. Redweik, M. C. Brito, Modelling solar potential in the urban environment: State-of-the-art review, Renewable and Sustainable Energy Reviews 41 (2015) 915–931. doi:10.1016/j.rser.2014.08.060.

[28] P. Ineichen, J. M. Gremaud, O. Guisan, A. Mermoud, Study of the corrective factor involved when measuring the diffuse solar radiation by use of the ring method, Solar Energy 31 (1) (1983) 113–117. doi:10.1016/0038-092X(83)90041-5.

[29] S. A. M. Burek, B. Norton, S. D. Probert, Analytical and experimental methods for shadow-band correction factors for solarimeters on inclined planes under isotropically diffuse and overcast skies, Solar Energy 40 (2) (1988) 151–160. doi:10.1016/0038-092X(88)90084-9.

[30] J. Rakovec, K. Zaksek, On the proper analytical expression for the sky-view factor and the diffuse irradiation of a slope for an isotropic sky, Renewable Energy 37 (1) (2012) 440–444. doi:10.1016/j.renene.2011.06.042.

[31] K. M. Ng, N. M. Adam, O. Inayatullah, M. Z. A. A. Kadir, Assessment of solar radiation on diversely oriented surfaces and optimum tilts for solar absorbers in Malaysian tropical latitude, International Journal of Energy and Environmental Engineering 5 (1) (2014) 5. doi:10.1186/2251-6832-5-5.

[32] E. G. Evseev, A. I. Kudish, An assessment of a revised Olmo et al. model to predict solar global radiation on a tilted surface at Beer Sheva, Israel, Renewable Energy 34 (1) (2009) 112–119. doi:10.1016/j.renene.2008.04.012.

[33] D. T. Reindl, W. A. Beckman, J. A. Duffie, Diffuse fraction correlations, Solar Energy 45 (1) (1990) 1–7. doi:10.1016/0038-092X(90)90060-P.

[34] A. P. Brunger, F. C. Hooper, Anisotropic sky radiance model based on narrow field of view measurements of shortwave radiance, Solar Energy 51 (1) (1993) 53–64. doi:10.1016/0038-092X(93)90042-M.

[35] A. I. Kudish, E. G. Evseev, The assessment of four different correction models applied to the diffuse radiation measured with a shadow ring using global and normal beam radiation measurements for beer sheva, israel, Solar Energy 82 (2) (2008) 144–156. doi:10.1016/j.solener.2007.06.006.

13

Highlights for "New device for the simultaneous measurement of diffuse solar irradiance on several azimuth and tilting angles"

- A review of the most commonly used solar diffuse measurement systems was made.

- A new device for the measurement of diffuse irradiance is presented.

- The presented device is based on an innovative single multi-lobe shadowband.

- A geometrical correction factor for measurements is calculated for all positions.

- Acurate and reliable performance have been observed on preliminary results.

1